CRYSTALLOGRAPHY REPORTS, 2025, Vol. 70, No. 1, pp. 70–79

PHYSICAL PROPERTIES OF CRYSTALS

STUDY OF $Pb_{0.5}Cd_{0.25}Lu_{0.25}F_{2.25}$ FLUORITE SOLID SOLUTION WITH CONGRUENT MELTING NATURE

© 2025 I. I. Buchinskaya*, M. V. Koldaeva, N. I. Sorokin, A. G. Kulikov, and D. N. Karimov

Shubnikov Institute of Crystallography, Kurchatov Complex of Crystallography and Photonics, National Research Centre "Kurchatov Institute", Moscow, Russia

**e-mail: buchinskayii@gmail.com*

Received August 15, 2024
Revised September 15, 2024
Accepted September 17, 2024

Abstract. For the first time, the optical, mechanical and conductive properties of the $Pb_{0.5}Cd_{0.25}Lu_{0.25}F_{2.25}$ crystalline matrix were studied in comparison with the crystals of the initial single-component fluorides. The short-wavelength transparency boundary of the three-component mixed crystal is determined by the presence of PbF_2 in its composition, the IR boundary is naturally shifted up to 15 μm due to the presence of LuF_3 in the composition. The refractive index of the studied solid solution $n = 1.6889$ on the $\lambda = 0.6328$ μm wavelength is lower than that of the PbF_2 crystal due to the introduction of less polarizable components CdF_2 and LuF_3. For the three-component crystal, significant strengthening is observed, the microhardness $H_V = 2.5$ GPa, which exceeds the hardness values of PbF_2 and CdF_2 by almost 40 %. The electrical conductivity of $Pb_{0.5}Cd_{0.25}Lu_{0.25}F_{2.25}$ σ_{dc} at 500 K is 5.5×10^{-5} S/cm, which corresponds to the conductivity level of solid solutions $M_{1-x}Lu_xF_{2+x}$ (M = Ca, Sr, Ba). The studied multicomponent fluoride material can be a promising crystalline medium for various photonic applications.

DOI: 10.31857/S00234761250110e7

INTRODUCTION

Materials based on metal difluorides MF_2 (M = Ca, Sr, Ba, Pb, Cd) with a fluorite structure are actively used in various fields of science and technology as polyfunctional crystalline elements [1, 2], which is ensured by the ease of obtaining bulk MF_2 crystals and their high isomorphic capacity with respect to rare earth element (**REE**) ions, transparency in a wide spectral range, unique spectroscopic characteristics, chemical stability, etc. The practical use of simple MF_2 often encounters limitations in the design of optical and laser systems associated with the lack of variability in the functional characteristics of these materials [3], therefore, significant modification of the chemical composition and the transition to multicomponent concentrated (binary and ternary) solid solutions based on MF_2 are an effective way to ensure a variety of physicochemical properties of fluorite crystalline matrices and expand the range of available materials with the required performance parameters.

However, on the one hand, the use of solid solutions allows for significant modification of the basic characteristics inherent in fluorides, on the other hand, most solid solutions melt/solidify incongruently, which creates limitations in obtaining a chemically homogeneous crystalline material. Incongruently solidifying crystals are best grown from their own melt using directional crystallization methods with feeding, which creates technological difficulties. Therefore, of particular interest from the point of view of the homogeneity of the chemical composition and, accordingly, the constancy of properties are multicomponent compositions that have a congruent melting character, which correspond to the extreme points of the phase diagrams – temperature minima, maxima and saddles on the lines or surfaces of the liquidus and solidus [4].

Recently, there has been a surge in research activity in relation to crystalline optical matrices CdF_2 [5–7] and PbF_2 [8–10], as well as optical ceramics and glasses with their participation. Despite the generally recognized environmental hazard of lead and cadmium fluorides, materials based on them provide high values of density, refractive indices and radiation resistance while maintaining the broadband transparency window and isomorphic capacitance characteristic of MF_2 fluorides. In addition, PbF_2 and $Pb_{0.67}Cd_{0.33}F_2$ crystals have high fluorine-ion conductivity [11–13].

The search for congruently melting compositions in the PbF_2–CdF_2–RF_3 (R = Tb, Ho, Er, Tm, Yb, Lu) systems was carried out earlier; in [14], a series of crystals $(Pb_{1-y}Cd_y)_{1-x}R_xF_{2+x}$ was obtained by the directional crystallization method and it was shown that for the $Pb_{0.5}Cd_{0.25}Lu_{0.25}F_{2.25}$ sample, the axial

distribution coefficients of the components, estimated by the X-ray spectrometry method, are practically equal to unity. This fact makes this solid solution very attractive for the crystallization of homogeneous material by melt methods.

The possibilities of using the material as a functional crystalline matrix largely depend not only on its optical but also on its mechanical characteristics. Note that the mechanical properties of multicomponent fluorides have been little studied. Therefore, the purpose of this work is to study a number of physical properties of the $Pb_{0.5}Cd_{0.25}Lu_{0.25}F_{2.25}$ crystal to assess the range of its functionality and potential for practical application.

The features of growing a solid solution of $Pb_{0.5}Cd_{0.25}Lu_{0.25}F_{2.25}$ by the method of spontaneous vertical directional crystallization (Bridgman–Stockbarger) in a fluorinating atmosphere are described in [14].

Fig. 1a shows a fragment of the liquidus surface of the ternary system PbF_2–CdF_2–LuF_3 with a region of the fluorite solid solution $Pb_{1-x-y}Cd_xLu_yF_{2+y}$ and melting temperatures of the compositions corresponding to special points. The crystallization progress lines obtained from thermodynamic-topological analysis [14] are schematically plotted on it.

Further studies were carried out on a sample cut along the growth axis and polished to optical quality (Fig. 1b).

CHARACTERIZATION OF CRYSTAL BY X-RAY METHODS

X-ray phase analysis (**XRD**) was performed on a Rigaku MiniFlex 600 powder diffractometer (CuK_α-radiation) in the range $2\theta = 10°$–$120°$, he lattice parameter of the solid solution was refined by full-profile analysis using the Le Bail method [15] in the sp. gr. using the Jana2006 program [16].

According to the XRD results, the studied sample of the $Pb_{0.5}Cd_{0.25}Lu_{0.25}F_{2.25}$ composition is single-phase and has a fluorite structure. The diffraction pattern of the crystal is shown in Fig. 2. The lattice parameter $a = 5.6928(2)$ Å is constant along the length of the crystal within the measurement error. The lattice parameter of the crystal occupies an intermediate position between the parameters of the PbF_2 and CdF_2 components, the high density is maintained due to the introduction of the heavy component LuF_3 into the composition.

Cubic crystals of the MF_2 type (M – alkaline earth metals) are easily crystallized from the melt by the seedless method. Numerous experiments on growing CaF_2 by the Bridgman method in crucibles with a flat bottom (method of the Vavilov State Optical Institute) have shown that there is a tendency for the crystals to be predominantly oriented in directions close to <110> [17].

The orientation of the studied crystal plate and determination of the degree of its structural perfection were performed on a TRS-K three-crystal diffractometer equipped with a molybdenum X-ray tube with a wavelength of $\lambda = 0.70932$ Å ($MoK_{\alpha1}$ radiation). A highly perfect Si 220 crystal served as a monochromator. After the monochromator, a slit aperture with a variable cross-section was installed, limiting the projection area of the X-ray beam on the sample. The dimensions of the slit aperture were 6.0×0.2 and 2.5×0.2 mm^2. A Radicon SCSD-4 point scintillation detector was used to record the diffracted X-ray radiation.

Orientation analysis showed that the $Pb_{0.5}Cd_{0.25}Lu_{0.25}F_{2.25}$ crystal grew in the direction at an angle of ~12 relative to the <111> axis. The studied plate had a surface orientation close to the crystallographic

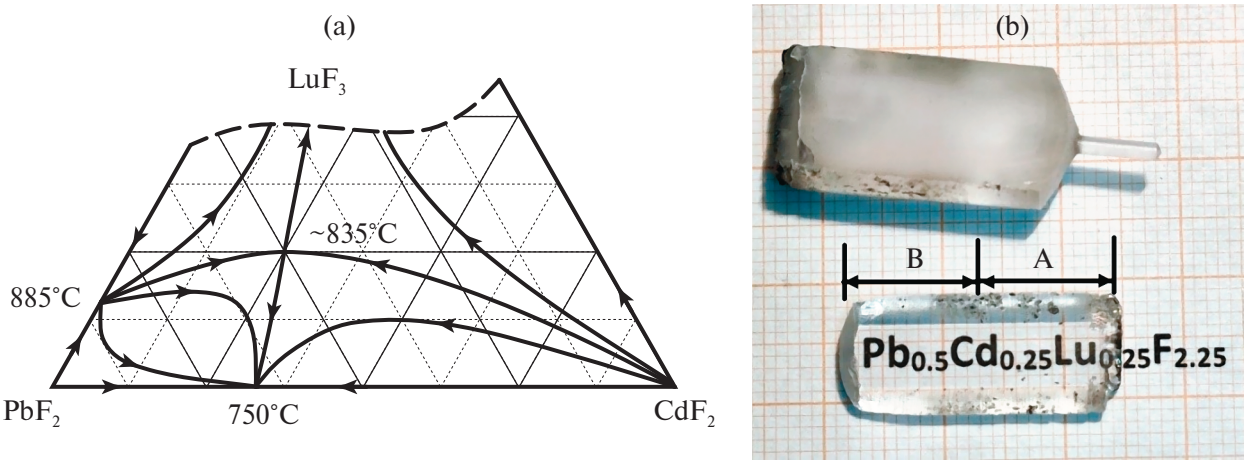

Fig. 1. Region of solid solution with congruent melting character (saddle point) on concentration triangle PbF_2–CdF_2–LuF_3 (a). Arrows schematically show the course of crystallization lines on the liquidus surface. External view of crystalline boule $Pb_{0.5}Cd_{0.25}Lu_{0.25}F_{2.25}$ and plate polished for research (b).

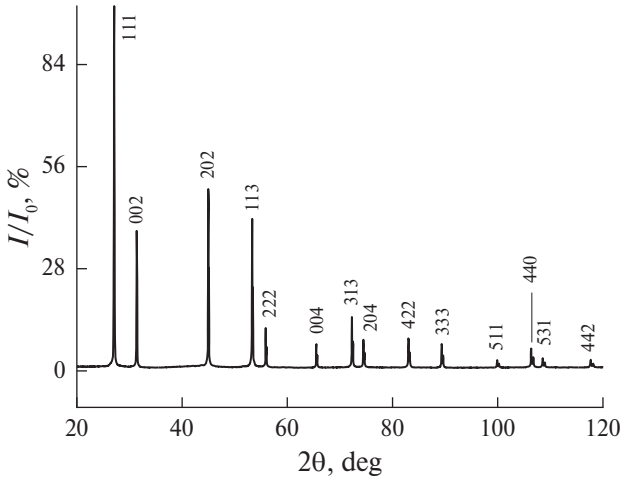

Fig. 2. Diffraction pattern of $Pb_{0.5}Cd_{0.25}Lu_{0.25}F_{2.25}$ powder.

plane {211} (Fig. 3a) with a deviation of 2.5 relative to the normal.

The structural perfection of the sample was assessed using the 422 reflection with a Bragg angle of 16.89 (for Mo$K_{\alpha 1}$ radiation). The diffraction reflection curve has many satellites corresponding to a fine-block crystal structure with an angular misorientation in the range of 30–40 arc min (Fig. 3b).

For the studies, uniformly quenched, unstressed sections of the crystal were selected (Fig. 4).

MECHANICAL PROPERTIES

Vickers microhardness H_V was measured by the standard microindentation method on a KV-10 hardness tester (Germany) depending on the applied load P. Indentation was carried out in groups of five prints with a fixed load P. The distance between the prints was 150–250 μm depending on the load. Both diagonals of the print (d_1, d_2) were measured, and the microhardness HV was calculated using the formula [18]:

$$H_V\ [\text{kgf/mm}^2] = 1.854\ P/d_m^2, \qquad (1)$$

where $d_m = (d_1 + d_2)/2$. Further, all units of measurement are expressed in the SI system.

Fig. 5 shows a typical indentation made at $P = 0.5$ N and a diagram of the measured values. It can be seen that the indentation process is accompanied by the formation of cracks around the indentation. The orientation of the indenter relative to the sample surface for characterizing its crack resistance was selected so that the cracks of length c formed during indentation originated from the corners of the indentation. Averaging for the $H(P)$ and $c(P)$ dependencies was performed over five indentations and 20 cracks, respectively. The effective Young's modulus E, as well as the microhardness HB, were measured by the instrumental indentation method [19] on a Nanoscan 4D nanohardness tester with a Berkovich pyramid and were also averaged over five measurements for each of the loads. Fracture toughness

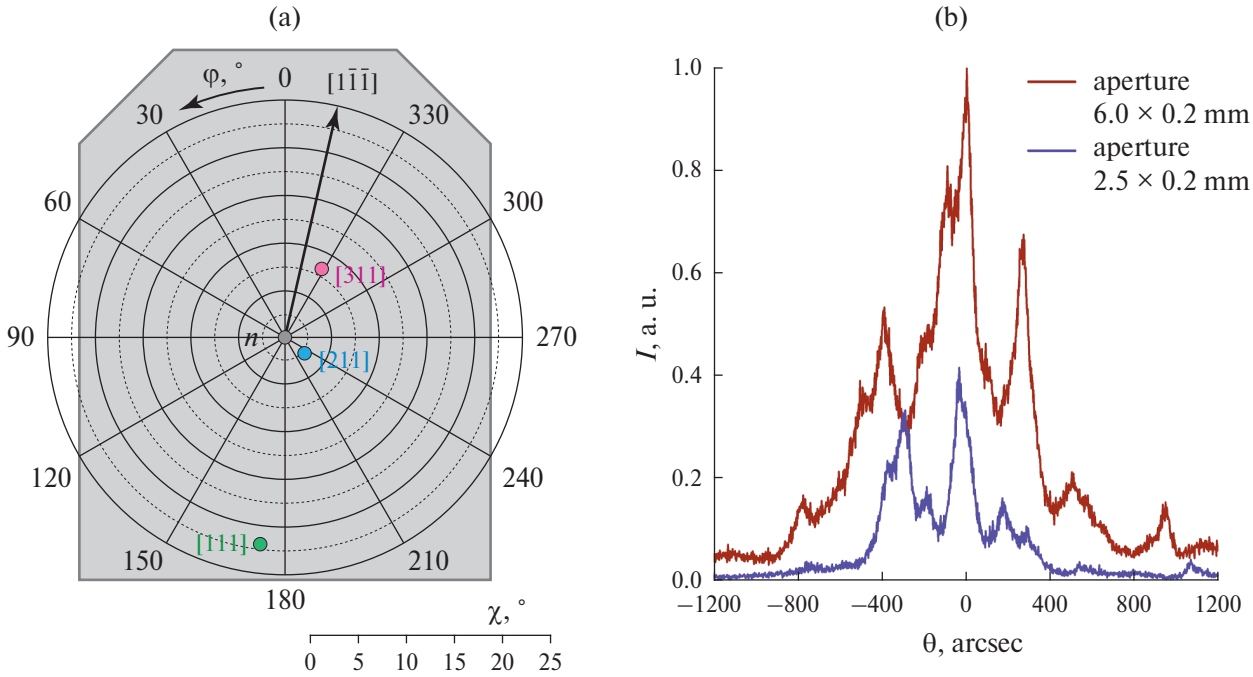

Fig. 3. Scheme of crystallographic directions relative to the studied crystal plate (a). Diffraction reflection curves obtained on reflection 422 (b).

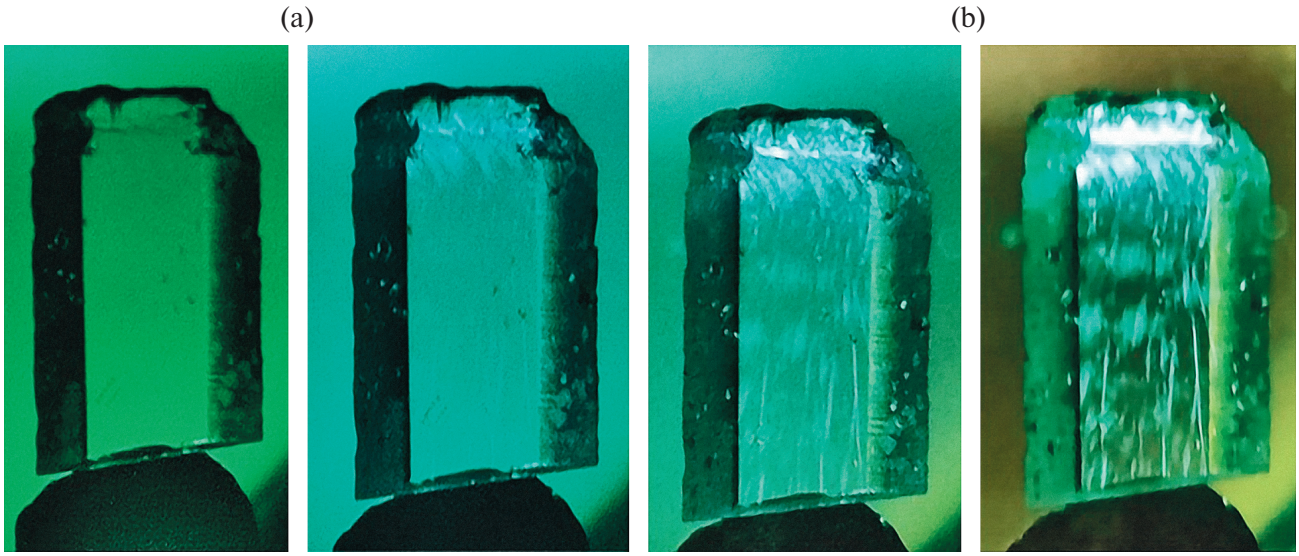

Fig. 4. Conometric images of the sample in polarized light. The angle between the polaroids varies from 0° (a) to 90° (b).

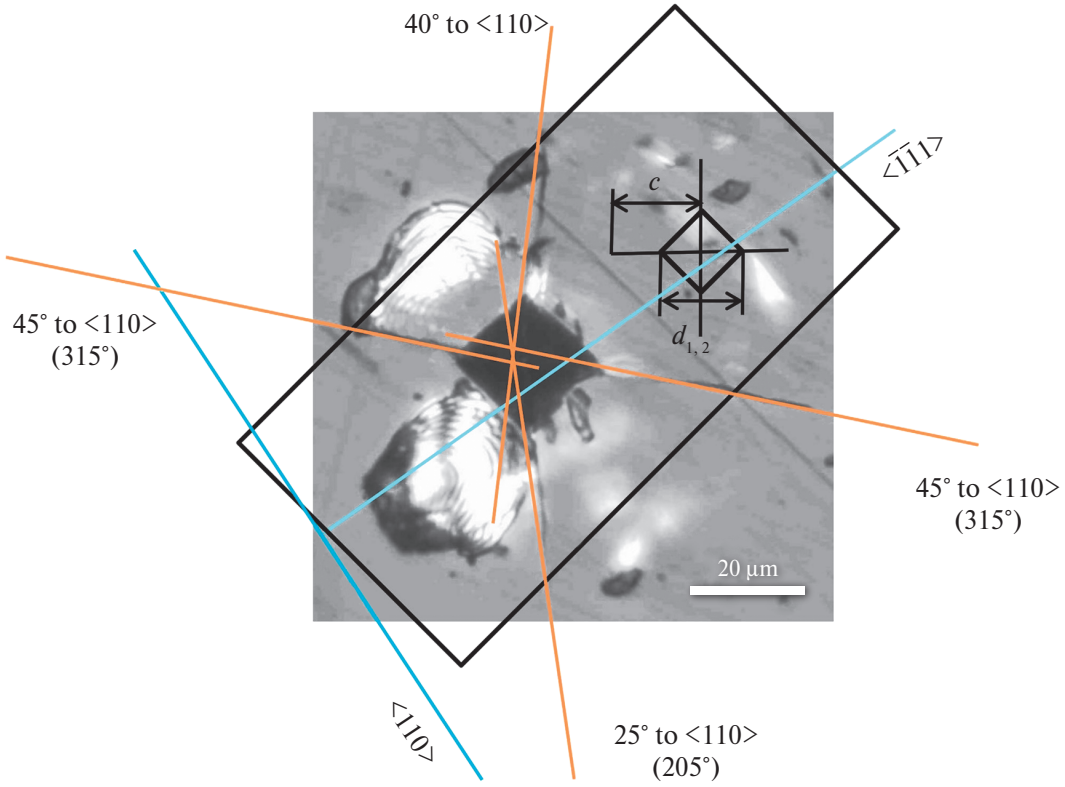

Fig. 5. Photograph of the indenter imprint at $P = 0.5$ N and schematic representation of the measured lengths of the diagonals d_1, d_2 and cracks c.

K_C was calculated using the formula for radial (half-disk or half-penny) cracks along the indenter edges [20]:

$$K_C = (0.016 \pm 0.004)\sqrt{E/H}\left(P/c^{3/2}\right). \quad (2)$$

The mechanophysical characteristics were measured for comparison on the lower (A) and upper (B) parts of the sample (Fig. 1b) (with a conditional division of the plate area in half) at $P = 0.5$ N for 20 prints in each zone.

The mechanical properties of MF_2 fluorides and solid solutions based on them have not been systematically studied to date, with the exception of CaF_2 and BaF_2 crystals, which is due to their widespread use in the optical industry.

The hardness and fracture toughness of CaF_2 crystals, studied by nano- and microindentation methods, and determination of Young's modulus by resonance acoustic spectroscopy are presented in [21]. It is noted that the Knoop hardness and Young's modulus largely depend on the orientation of the CaF_2 crystal, while the Vickers hardness and fracture toughness are orientation-independent. At a load of $P = 200$ gf (1.96 N), the Vickers hardness for the CaF_2 crystal is 1.98 GPa, and the fracture toughness is 0.7 MPa·m$^{1/2}$.

In [22], it is shown that the maximum value of the Vickers hardness of CaF_2 is 1.67 GPa. The value of Young's modulus, measured by the method of instrumental indentation along the [111] direction, is 89.6 GPa, the fracture toughness is 0.7 MPa·m$^{1/2}$. In [23], the microhardness and fracture toughness of a single crystal of the $Ca_{0.97}Yb_{0.03}F_{2.03}$ solid solution were studied. Its microhardness increases with the introduction of the Yb^{3+} impurity and is 2.95 ± 0.07 GPa; the fracture toughness is 0.45 ± 0.1 MPa m$^{1/2}$.

Microhardness and fracture toughness for concentration series of fluorite solid solutions based on CaF_2 with R = Tm, Ho [24] based on SrF_2 with R = La, Nd, Sm, Gd, Ho, Er–Lu, Y) [25] were investigated without reference to crystallographic directions. In [24], the microhardness for CaF_2 is given as 1.63 ± 0.03 GPa. The introduction of REE ions increases the microhardness values of CaF_2 to 2.5 and 2.8 GPa for R = Tm and Ho, respectively, and the fracture toughness value remains virtually unchanged. In [25], the microhardness for SrF_2 is 1.5 GPa, the introduction of REE impurity nonlinearly increases this value, the highest hardness (4.3 GPa) was obtained for the limiting solid solutions with R = La, Nd, and Gd. In [26], the results of a study of the microhardness of the three-component solid solution $Ca_{0.70}Sr_{0.24}Yb_{0.06}F_{2.06}$ are presented: 494 and 438 kgf/mm^2 (4.84 and 4.29 GPa) for $P = 40$ and 50 gf (0.39 and 0.49 N), respectively.

In [27], the microhardness of crystals of solid solutions $Ca_{0.77}Sr_{0.07}La_{0.16}F_{2.16}$ and $Ca_{0.70}Sr_{0.11}Ce_{0.19}F_{2.19}$ was investigated and a significant strengthening of three-component crystals was shown in comparison with one- and two-component ones.

The presented data indicate that the transition to multicomponent solid solutions (alloying) is accompanied by an increase in the hardness of crystals and a decrease in their crack resistance.

The available data on microhardness for crystals of CdF_2, PbF_2 and solid solutions based on them are ambiguous. According to [28], the Vickers microhardness measured on the (111) face for crystals of CdF_2 and PbF_2 is 1.53 and 1.33 GPa, respectively, and according to [29], for the isovalent solid solution $Pb_{0.67}Cd_{0.33}F_2$ ~1.47 GPa. This value is intermediate, but it is possibly underestimated, since the measurements were carried out on a sample of arbitrary orientation, whereas there is an orientation dependence of microhardness (the (111) plane in the fluorite structure is close-packed and the hardest).

In this paper, the microhardness and Young's modulus studies were performed for a $Pb_{0.5}Cd_{0.25}Lu_{0.25}F_{2.25}$ plate with a surface orientation close to the (211) plane (Fig. 4a). When indenting with a Vickers pyramid, it was found that crystallographically oriented cracks formed near the imprint. Therefore, the working surface of the sample was turned relative to the indenter so that the cracks emerged strictly from the vertices of the imprint. In this case, the angle between the diagonal of the indenter imprint and the long edge of the sample was ~45° (Fig. 5).

In Fig. 6a, the triangular symbols show the dependence of the Vickers microhardness H_V on the load $P = 0.5$ N. The average standard deviation of ±3.5 %, typical for most measurements, is set as the relative error. The range of standard deviations for each of the samples was ±5 %. The round symbols in Fig. 6a designate the dependence of the microhardness measured by the instrumental indentation method with the Berkovich triangular pyramid. A special feature of this method is that the microhardness H_B and the effective Young's modulus E are determined from the curves of the indenter penetration depth as a function of the load during the indentation process (the Oliver-Pharr method) [19]. During statistical processing, the results where the prints were formed with cracks were excluded. Apparently, this is why the H_B values exceed the H_V microhardness values over the entire range of loads. The range of indentation loads for H_B measurements is smaller than for H_V, since it becomes impossible to perform indentation without cracking. In addition, a stronger drop in H_V hardness values with increasing load may also be associated with more active crack formation.

When indented with a Vickers pyramid, developed half-penny cracks are formed, emerging on the sample surface from the corners of the indentation. Measuring their length $c(P)$, microhardness $H(P)$ and $E(P)$ using formula (2), we calculated the fracture toughness coefficient (K_C), which characterizes the crack resistance of the crystal (Fig. 6b). It is evident that starting from $P = 0.3$ N, the K_C value ceases to depend on the load, reaching an average value of 0.257 ± 0.017 MPa·m$^{1/2}$ in the range of $0.3 < P < 3$ N. At lower loads, the condition $c/a < 2.5$ ($a = d/2$) is met, which gives overestimated K_C values.

Quite a large scatter of microhardness values is possibly due not only to brittle fracture of the crystal during indentation, but also to structural imperfection of the sample. Moreover, standard deviations of H_B and H_V values are on average the same and practically do not depend on the load, although they are measured

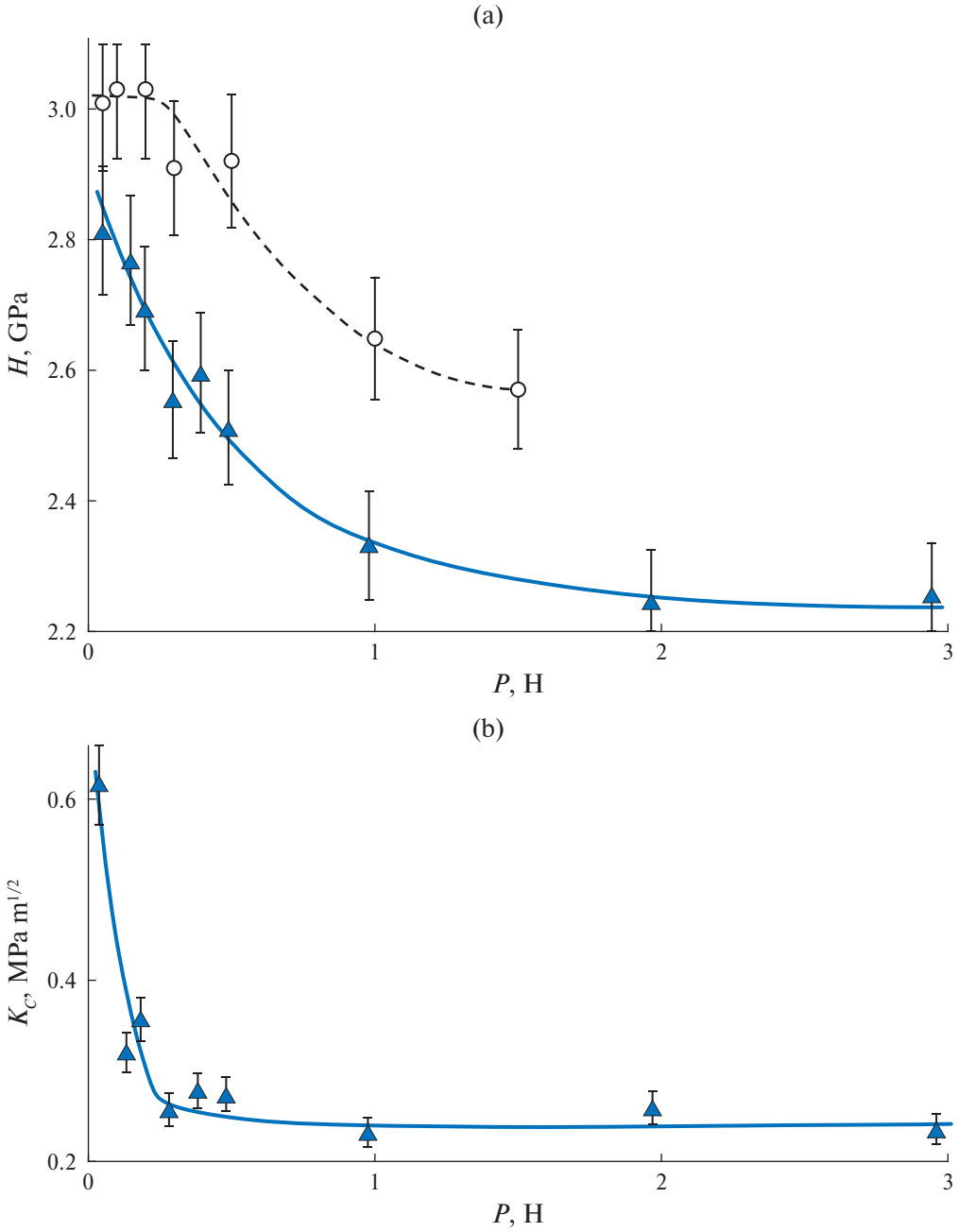

Fig. 6. Dependences of microhardness (a) and fracture toughness coefficient (b) on the indenter load. Triangular symbols indicate microhardness according to Vickers, round symbols indicate measurement by the instrumental indentation method using the Berkovich pyramid.

in different ways – excluding crack formation in the first case and with the formation of developed cracks in the second. Table 1 shows the results of comparative measurements of mechanical characteristics in areas A and B on different parts of the sample, at $P = 0.5$ N for 20 indentations in each zone A and B. These areas of the sample differ in their perfection. As can be seen in polarized light (Fig. 4), area B contains more stressed areas. Obviously, despite the differences in the crystal areas, the Vickers microhardness value $H_V = 2.5$ GPa was obtained with good repeatability for different parts of the plate. Effective Young's modulus $E = 91.7$ GPa. The difference in the average values of all mechanical characteristics in areas A and B does not exceed the standard deviation, which indicates high homogeneity of the sample.

As shown above, the introduction of a rare earth impurity into CaF_2 is accompanied by an increase

Table 1. Vickers microhardness H_V, crack length c, Young's modulus E and fracture toughness K_C measured at $P = 0.5$ N for sample sections A and B (Fig. 1b)

	H_V, GPa	c, μm	E, GPa	K_C, MPa m$^{1/2}$
Average A	2.511	30.95	90.65	0.277
Average B	2.490	29.49	92.83	0.296
(B–A)/A, %	–3.95	–4.72	2.40	6.86
Standard deviation σ_A	0.087	3.77	2.37	
Relative deviation σ_A, %	3.46	12.18	2.61	

in microhardness, on the one hand, and a decrease in crack resistance, on the other. There is reason to believe that this trend is also observed in the case of the $Pb_{0.5}Cd_{0.25}Lu_{0.25}F_{2.25}$ crystal. The formation of a heterovalent solid solution based on fluorite is accompanied by clustering with an increase in the packing density of the structure [30]. Obviously, this is why the crystal is strengthened with a simultaneous increase in its brittleness (decrease in crack resistance).

Thus, the studied crystal can be classified as a group of solid materials prone to brittle fracture.

OPTICAL RESEARCH

The refractive index n of the $Pb_{0.5}Cd_{0.25}Lu_{0.25}F_{2.25}$ crystal was measured at a wavelength of $\lambda = 0.6328$ μm at $T = 293$ K using a Prism Coupler System Metricon 2010/M (Metricon Corp., USA). The measurement technique is described in detail in [31].

The refractive index of the studied solid solution is lower than that of the pure PbF_2 matrix due to the introduction of less polarizable components CdF_2 and LuF_3, due to which it occupies an intermediate position between PbF_2 and CdF_2 (Table 2).

Transmission spectra were recorded using a Cary-5000 spectrophotometer (Agilent Technologies) and an FTIR-8100 Fourier transform IR spectrometer (Shimadzu) at room temperature in the wavelength range $\lambda = 0.2$–15 μm.

The transmission spectra of the $Pb_{0.5}Cd_{0.25}Lu_{0.25}F_{2.25}$ sample and a number of crystals based on PbF_2 and CdF_2 [17] are shown in Fig. 7 for comparison. The nominally pure PbF_2 sample (curve *3*) is transparent in the range from 0.24 to 14 μm, which corresponds to the data of [33–36].

Of the presented objects, cadmium fluoride (curve *4*) is the most transparent in the short-wave range down to 0.2 μm. The observed selective absorption in the 0.22 μm region is due to the presence of Pb^{2+} ions in these crystals [37]. The introduction of CdF_2 ions into the Lu^{3+} matrix significantly shifts the transmission boundary to the red region of the spectrum (curve *5*). The low transmission level of samples 1–3 is due to their optical processing under conditions of different humidity for hydrolyzing

Table 2. Lattice parameter a, X-ray density ρ_x and refractive index n for some fluoride crystals with fluorite structure

Crystal composition	a, Å	ρ_x, g/cm^3	n at $\lambda = 0.6328$ μm
$Pb_{0.5}Cd_{0.25}Lu_{0.25}F_{2.25}$	5.6928(2)	7.85	1.6889
$Pb_{0.67}Cd_{0.33}F_2$	5.7317(3)	7.52	1.7049 [31]
PbF_2	5.939(4)	7.77	1.7611 [31]
CdF_2	5.388(2)	6.38	1.5726 [32]

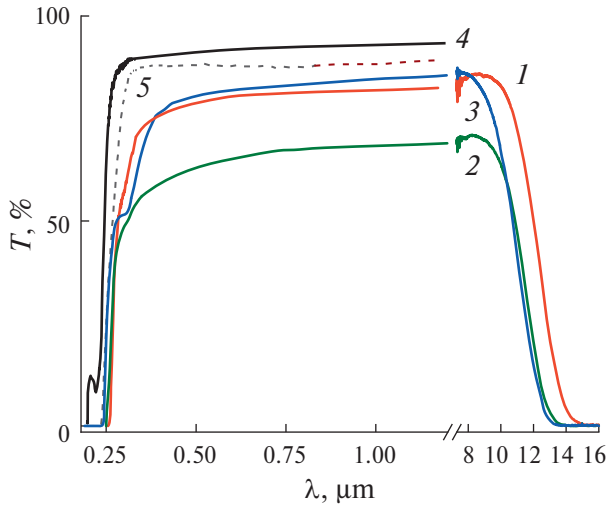

Fig. 7. Transmission spectra of $Pb_{0.50}Cd_{0.25}Lu_{0.25}F_{2.25}$ (1), $Pb_{0.621}Cd_{0.3}Sr_{0.079}F_2$ (2), PbF_2 (3), $Cd_{0.9}Lu_{0.1}F_{2.1}$ (4) and CdF_2 (5) crystals. Sample thickness is 2 mm.

fluoride crystals. The additional observed absorption in the 0.3 μm region is due to the uncontrolled content of Ce^{3+} ions [35].

The transmission limit of the $Pb_{0.5}Cd_{0.25}Lu_{0.25}F_{2.25}$ (curve *1*) in the UV range is determined by the presence of PbF_2 in its composition and practically coincides with the optical data for the $Pb_{0.621}Cd_{0.3}Sr_{0.079}F_2$ (curve *2*) and $Cd_{0.9}Lu_{0.1}F_{2.1}$ (curve *5*). The presence of PbF_2 in the composition of multicomponent matrices leads to an

insignificant red shift of the short-wave transmission limit [36]. The transmission limit of the studied crystal in the IR region of the spectrum is regularly shifted to the long-wave side (up to 15 μm) due to the presence of heavy LuF_3 in the composition.

ELECTRICALLY CONDUCTIVE PROPERTIES

Direct current *electrical conductivity* was measured by impedance spectroscopy. The sample of the $Pb_{0.5}Cd_{0.25}Lu_{0.25}F_{2.25}$ solid solution was a rectangular parallelepiped 2 × 5 × 5 mm, the smallest edge of which was directed along the crystal growth axis. Electrophysical measurements of the sample were carried out in two mutually perpendicular directions: along and across the crystal growth axis. For this purpose, inert electrodes (Leitsilber silver paste) were applied to the working surfaces of the sample. The complex impedance $Z^*(w) = Z' + iZ''$ (i s the imaginary unit) of the Ag|crystal|Ag electrochemical system was measured in the frequency ranges of 5–5 × 10^5 Hz and resistances of 1–10^7 Ohm (Tesla BM–507 impedance meter) in a vacuum of ~1 Pa in the temperature range of 378–818 K in the cooling mode. The relative measurement error of $Z^*(w)$ did not exceed 5 %. The impedance measurement technique is described in detail in [38].

The volume resistance R_{crys} of the crystal was found from the frequency dependences of the complex impedance of the electrochemical cells $Ag|Pb_{0.5}Cd_{0.25}Lu_{0.25}F_{2.25}|Ag$ by the intersection of the impedance hodograph with the axis of active resistances. The specific electrical conductivity σ_{dc} was calculated using the formula:

$$\sigma_{dc} = h/(R_{crys}S), \quad (3)$$

where h is the sample thickness, S is the electrode area.

As mentioned above, fluorite solid solutions based on PbF_2 have fluorine-ion conductivity. The ionic conductivity values measured along and across the crystal growth axis coincide with each other, so the conductometric data were further processed jointly. The generalized temperature dependence of the ionic conductivity $\sigma_{dc}(T)$ or the fluorite solid solution $Pb_{0.5}Cd_{0.25}Lu_{0.25}F_{2.25}$ is shown in Fig. 8. The $\sigma_{dc}(T)$ ependence does not have any features; in the studied temperature range of 378–818 K, the σ_{dc} alue increases linearly from 2.0 × 10^{-7} to 4.9 × 10^{-2} S/cm (by 2.5 × × 10^5 times).

The temperature dependence of conductivity was processed in accordance with the Arrhenius–Frenkel equation:

$$\sigma_{dc}T = A\exp(-\Delta H_\sigma/kT), \quad (4)$$

where A is the pre-exponential factor of electrical conductivity and ΔH_σ is the activation enthalpy of ion transfer. The experimental data satisfy the Arrhenius–Frenkel equation with fitting parameters A = 2.55 × 10^6 SK/cm and ΔH_σ = 0.791 ± 0.005 eV, respectively. The value od σ_{dc} at 500 K is 5.5 × 10^{-5} S/cm.

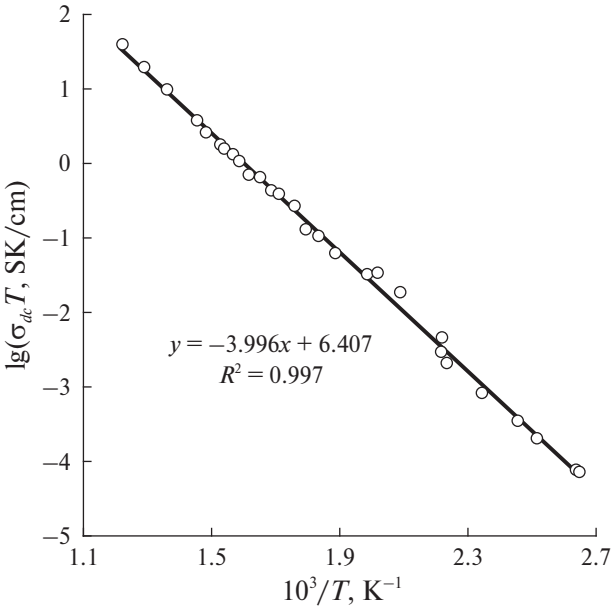

Fig. 8. Temperature dependence of ionic conductivity of the $Pb_{0.5}Cd_{0.25}Lu_{0.25}F_{2.25}$ solid solution crystal: circles – experiment, straight line – approximation of experimental data by a linear equation ($x = 10^3/T$, $y = \lg(\sigma_{dc}T)$, R – correlation coefficient).

When introducing LuF_3 impurity, excess fluorine anions are localized in the interstitial positions of the fluorite matrices PbF_2 and CdF_2 in accordance with the quasi-chemical reaction:

$$LuF_3\,(PbF_2, CdF_2) \rightarrow Lu_{Pb,Cd} + F_i' + 2F_F^{\times}. \quad (5)$$

The designation of defects is given in Kroeger-Vink symbols [39].

The average value of potential barriers, equal to 0.79 eV, in $Pb_{0.5}Cd_{0.25}Lu_{0.25}F_{2.25}$ for interstitial ions F_i' participating in the ion transfer process is higher than the similar characteristic for fluorite solid solutions $Pb_{1-x}Lu_xF_{2+x}$, $Cd_{1-x}Lu_xF_{2+x}$, but is comparable or lower for solid solutions $M_{1-x}Lu_xF_{2+x}$ (M = Ca, Sr, Ba) (Table 3).

CONCLUSION

For the first time, a comprehensive characterization of the multicomponent congruently melting solid solution $Pb_{0.5}Cd_{0.25}Lu_{0.25}F_{2.25}$ was carried out. The crystal is a strong, high-density and highly refractive optical material with a wide transparency window. The search, synthesis and study of multicomponent fluoride materials of variable composition determine the direction for further expansion and modification of the range of physical properties for specific applied tasks.

Table 3. Sample type, production method and ionic conductivity of fluorite solid solutions based on MF_2 (M = Ca, Sr, Ba, Cd, Pb) and LuF_3

Composition/Type of sample	Method of obtaining	σ_{dc}, S/cm T = 500 K	ΔH_σ, eV	References
$Pb_{0.5}Cd_{0.25}Lu_{0.25}F_{2.25}$ monocrystal	Directional crystallization of melt	5.5×10^{-5}	0.79	This work
β-PbF_2 monocrystal		2.5×10^{-4} 3.5×10^{-4} 3.5×10^{-4} 8.6×10^{-5}	0.66 0.72 1.05 1.04	[40] [41, 42] [43] [44]
$Pb_{0.9}Lu_{0.1}F_{2.1}$ polycrystal	Melting	3.3×10^{-3}	0.42	[41]
$Cd_{0.83}Lu_{0.17}F_{2.17}$ monocrystal	Directional crystallization of melt	8.0×10^{-5}	0.64	[45]
$Ca_{0.75}Lu_{0.25}F_{2.25}$ monocrystal		9.5×10^{-8}	0.91	[9, 46]
$Sr_{0.75}Lu_{0.25}F_{2.25}$ monocrystal		3.4×10^{-8}	1.08	[47]
$Ba_{0.85}Lu_{0.15}F_{2.15}$ monocrystal		2.2×10^{-5}	0.75	[48]

ACKNOWLEDGMENTS

The authors express their gratitude to A.G. Savelyev and B.V. Nabatov for assistance in obtaining experimental data, as well as to E.A. Petrzhik for participation in the discussion of the results.

FUNDING

The work was carried out within the framework of the state assignment of the National Research Center "Kurchatov Institute" using the equipment of the Center for Collective Use "Structural Diagnostics of Materials" of the Kurchatov Crystallography and Photonics Complex of the National Research Center "Kurchatov Institute".

CONFLICT OF INTERESTS

The authors declare no conflict of interest.

REFERENCES

1. *Mouchovski J.T., Temelkov K.A., Vuchkov N.K.* // Prog. Cryst. Growth Characteriz. Mater. 2011. V. 57. P. 1. https://doi.org/10.1016/J.PCRYSGROW.2010.09.003
2. *Fedorov P.P., Osiko V.V.* // Bulk Crystal Growth of Electronic, Optical and Optoelectronic Materials / Eds. Capper P. Hoboken; NJ; USA: John Wiley Sons, Ltd. 2005. P. 339. https://doi.org/10.1002/9780470012086.ch11
3. *Karimov D.N., Komarkova O.N., Sorokin N.I. et al.* // Crystallography. 2010. Vol. 55. No. 3. P. 556. https://doi.org/10.1134/S1063774510030247
4. *Fedorov P.P., Buchinskaya I.I.* // Advances in chemistry. 2012. V. 81. No. 1. P. 1. https://doi.org/10.1070/RC2012v081n01ABEH004207
5. *Bordj S., Satha H., Barros A. et al.* // Opt. Mater. 2021. V. 118. P. 111249. https://doi.org/10.1016/j.optmat.2021.111249
6. *Boubekri H., Fartas R., Diaf M. et al.* // Luminescence. 2024. V. 39. No. 4. P. e4719. https://doi.org/10.1002/bio.4719
7. *Cheddadi A., Fartas R., Diaf M., Boubekri H.* // J. Luminescence. 2024. V. 265. P. 120237. https://doi.org/10.1016/j.jlumin.2023.120237
8. *Tan J., Zhang P., Li Z., Chen Z.* // Infrared Phys. Technol. 2024. V. 140. P. 105391. https://doi.org/10.1016/j.infrared.2024.105391
9. *Wang Y., Jiang C., Zhang P. et al.* // J. Luminescence. 2019. V. 212. P. 160. https://doi.org/10.1016/j.jlumin.2019.04.038
10. *Huang X., Wang Y., Peixiong Z. et al.* // J. Alloys Compd. 2019. V. 811. P. 152027. https://doi.org/10.1016/j.jallcom.2019.152027
11. *Kavun V.Ya., Slobodyuk A.V., Goncharuk V.K., Lukiyanchuk G.D.* // Vestn. of the FEB RAS. 2009. No. 2. P. 117.
12. *Sorokin N.I.* // FTT. 2015. V. 57. No. 7. P. 1325.

13. *Trnovcova V., Fedorov P.P., Ozvoldova M. et al.* // J. Optoelectron. Adv. Mater. 2003. V. 5. P. 627.
14. *Buchinskaya I.I., Fedorov P.P.* // Crystallography. 2024. V. 69. No. 2. P. 353. https://doi.org/10.31857/S0023476124020194
15. *Le Bail A.* // Powder Diffraction. 2005. V. 20. P. 316. https://doi.org/10.1154/1.2135315
16. *Petricek V., Dusek M., Palatinus L.* // Z. Kristallogr. Cryst. Mater. 2014. B. 229. No. 5. P. 345. https://doi.org/10.1515/zkri-2014-1737
17. *Senguttuvan N., Aoshima M., Sumiya K., Ishibashil H.* // J. Cryst. Growth. 2005. V. 280. P. 462. https://doi.org/10.1016/j.jcrysgro.2005.03.085
18. *Mott B.W.* Micro-Indentation Hardness Testing. London, UK: Butterworths Scientific Publications, 1956.
19. *Oliver W.C.*, *Pharr G.M.* // J. Mater. Res. 2004. V. 19. No. 1. P. 3.
20. *Anstis G.R., Cbantikul P., Lawn B.R., Marsball D.B.* // J. Am. Ceram. Soc. 1981. V. 64. P. 533.
21. *Ladison J.L., Price J.J., Helfinstine J.D., Rosch W.R.* // Proc. SPIE. Optical Microlithography XVIII. 2005. V. 5754. P. 1329.
22. *Chen M., Jiang W., Cheng J., Chu X.* // Solid State Phenomena. 2011. V. 175. P. 77.
23. *Akchurin M.Sh., Basiev T.T., Demidenko A.A. et al.* // Opt. Mater. 2013. V. 35. No. 3. P. 444.
24. *Lyapin A.A.* // Spectral-luminescent properties of CaF_2:Tm, CaF_2:Ho single crystals and ceramics and their application in laser physics. Diss. ... Cand. Phys. and Mathematics. Saransk: FGBOU HPE Mordovian State University named after N.P. Ogarev, 2014. 142 p.
25. *Gryaznov M.Yu., Shotin S.V., Chuvildeev V.N. et al.* // Crystallography. 2012. V. 57. No. 1. P. 151.
26. *Kuznetsov S.V.* // Synthesis of single crystals and nanopowders of solid solutions of alkaline earth and rare earth metal fluorides for photonics. Diss. ... Cand. of Chemical Sciences. Moscow: MITHT, 2007. 206 p.
27. *Karimov D.N., Buchinskaya I.I., Sorokin N.I. et al.* // Crystallography. 2019. V. 64. No. 5. P. 831. https://doi.org/10.1134/S0023476119050102
28. *Kishan Rao K., Sirdeshmukh D.B.* // Bull. Mater. Sci. 1983. V. 5. P. 449.
29. *Buchinskaya I.I., Fedorov P.P., Sobolev B.P.* // Proc. SPIE 3178, Solid State Crystals: Growth and Characterization. 1997. V. 3178. P. 59. https://doi.org/10.1117/12.280705
30. *Sobolev B.P.* // Crystallography Reports. 2012. V. 57. No. 3. P. 434. https://doi.org/10.1134/S1063774512030194
31. *Buchinskaya I.I., Goryachuk I.O., Sorokin N.I. et al.* // Condens. Matter. 2023. V. 8. P. 73. https://doi.org/10.3390/condmat8030073
32. *Krukowska-Fulde B., Niemyski T.* // J. Cryst. Growth. 1967. V. 1. No. 4. P. 183. https://doi.org/10.1016/0022-0248(67)90051-6
33. *Guo-Hao Ren, Dingzhong Shen, Shaohua Wang, Zhiwen Yin* // J. Cryst. Growth. 2002. V. 243. P. 539. http://dx.doi.org/10.1016/S0022-0248(02)01579-8
34. *Guo-Hao Ren*, *Ding-Zhong Shen, Shao-Hua Wang, Zhi-Wen Yin* // Chinese Phys. Lett. 2001. V. 18. No. 7. P. 976. http://dx.doi.org/10.1088/0256-307X/18/7/344
35. *Ren G., Qun D., Li Z., Shen D.* // J. Cryst. Growth. 2003. V. 247. No. 1–2. P. 141. http://dx.doi.org/10.1016/s0022-0248(02)01952-8B
36. *Voronkova E.M., Grechushnikov B.N., Distler G.I., Petrov I.P.* Optical materials for infrared technology: Handbook. Moscow: Nauka, 1965. 336 p.
37. *Kosacki I., Langer J.M.* // Phys. Rev. B. 1986. V. 33. P. 5972(R). https://link.aps.org/doi/10.1103/PhysRevB.33.5972
38. *Sorokin N.I., Karimov D.N., Buchinskaya I.I.* // Electrochemistry. 2021. T. 57. No. 8. P. 465. https://doi.org/10.31857/S0424857021070136
39. *Kroger F.A., Vink H.J.* // Solid State Physics / Eds. Seitz F., Turnbull D. N.Y.: Academic Press, 1956. V. 3. P. 307.
40. *Bonne R.W., Schoonman J.* // Solid State Commun. 1976. V. 18. P. 1005.
41. *Sorokin N.I., Fedorov P.P., Sobolev B.P.* // Inorganic mater. 1997. V. 33. No. 1. P. 5.
42. *Popov P.A., Sidorov A.A., Kul'chenkov E.A. et al.* // Ionics. 2016. V. 23. No. 1. P. 223. https://doi.org/10.1007/s11581-016-1802-2
43. *Murin I.V., Glumov A.V., Glumov O.V.* // Electrochemistry. 1979. V. 15. No. 8. P. 1119.
44. *Bonne R.W., Schoonman J.* // J. Electrochem. Soc. 1977. V. 124. P. 28.
45. *Sorokin N.I., Fedorov P.P., Ivanov-Shits A.K., Sobolev B.P.* // FTT. 1988. V. 30. No. 5. P. 1537.
46. *Ivanov-Shits A.K., Sorokin N.I., Fedorov P.P., Sobolev B.P.* // Solid State Ionics. 1990. V. 37. P. 125.
47. *Ivanov-Shits A.K., Sorokin N.I., Fedorov P.P., Sobolev B.P.* // Solid State Ionics. 1989. V. 31. P. 253.
48. *Ivanov-Shits A.K., Sorokin N.I., Fedorov P.P., Sobolev B.P.* // Solid State Ionics. 1989. V. 31. P. 269.